Reducing Losses in Dielectric Waveguide Discontinuities

Robert Elio and El-Badawy El-Sharawy

***Abstract*— Rectangular dielectric waveguides are used in millimeter-wave applications. They have low loss and wide bandwidth at high frequencies. Another major advantage to dielectric waveguides is that they are inexpensive to design and manufacture. However, a major disadvantage to the dielectric waveguide is that they experience relatively high losses at bends and T-junctions. This paper looks at a novel approach in reducing the insertion loss in dielectric waveguide bends and T-junctions. A high dielectric material is inserted at the discontinuity, causing the electromagnetic energy to be coupled and launched toward the output. The dielectric constant of the material, position of the material, and shape of the material are instrumental in reducing the insertion loss. A transition discontinuity in the form of a 45° bend has also been found to reduce insertion loss when properly designed. The size, shape, and location of the discontinuity and the high dielectric material are optimized and compared to the results without a high dielectric material. The 90°- and 45°-bend simulations were verified by building test structures and comparing predictions of the insertion loss to measurements.**

***Index Terms*—Discontinuities, low-loss dielectric waveguide.**

I. Introduction

THE NEED for wide-band high-performance communication systems has led to the development of millimeter-wave devices. At millimeter-wave frequencies, conventional transmission lines exhibit high conductor losses, which reduce device gain and signal-to-noise ratio (SNR) [1]. Rectangular dielectric waveguides have very low loss in the millimeter-wave region and are easily interfaced to active circuits. They are easier to manufacture and are less expensive than metal waveguides [1], making them more practical. In monolithic circuit processing, reducing the amount of metal is very important in lowering the cost of the final product. The availability of high-permittivity and high-quality dielectric materials have made dielectric components feasible for applications in communications and broadcasting [1].

Although dielectric waveguides have many advantages, they exhibit very poor insertion loss and high reflection when a bend or T-junction is required. This disadvantage currently limits their widespread use [1]. To minimize the disadvantage introduced by these discontinuities, a novel approach is examined. The insertion loss is minimized by introducing a high-permittivity material at the discontinuity. This high dielectric material captures the electromagnetic energy and launches it toward the output. This concept has been investigated and reported in [1] for a single frequency to minimize the dielectric waveguide mode distortion. This paper reports the first study of the S-parameters of a dielectric waveguide discontinuity including high dielectric material over a wide band of frequencies. The dielectric constant, position, and shape of the material are instrumental in reducing the insertion loss. This paper also presents the effects of an optimized discontinuity in the form of a 45° bend. This type of bend has been found to reduce the insertion loss of dielectric discontinuity. Combining the effects of smooth discontinuity such as the 45° bend and the high dielectric material is also reported. Three cases are studied and optimized in detail: the 90° bend, the T-junction, and the 45° bend (see Fig. 1).

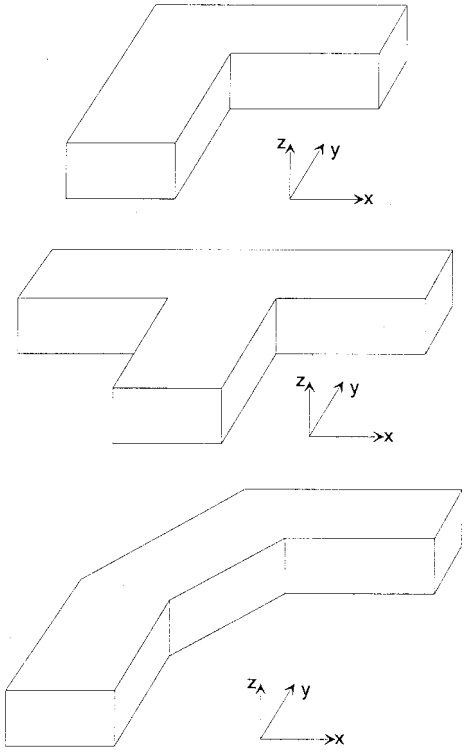

Fig. 1. Typical dielectric waveguide discontinuities.

Section II of this paper presents a simple transmission-line model of the dielectric bend. This model is used only to find the initial guess for the FDTD analysis, which is also presented in Section II. The results are discussed in Section III, and the loss analysis is verified experimentally in Section IV.

Manuscript received September 5, 1996; revised May 11, 1998.

R. Elio is with the Department of Electrical Engineering, College of Engineering and Applied Sciences, Arizona State University, Tempe, AZ 85287-7206 USA, and is also with the Semiconductor Products Sector, Motorola, Chandler, AZ 85224 USA.

E.-B. El-Sharawy is with the Department of Electrical Engineering, College of Engineering and Applied Sciences, Arizona State University, Tempe, AZ 85287-7206 USA.

Publisher Item Identifier S 0018-9480(98)05517-3.

A conclusion is presented, and future work is discussed in Section V.

II. Theory

A. Transmission-Line Model

To gain some insight into the effect that the high dielectric material has on the discontinuity, a simple transmission-line model is developed. This model provides an explanation of how the reflection from the discontinuity is reduced. The simplest case to develop a model for is the 90° bend (see Fig. 1). The corresponding transmission-line model is a simple three-section transmission line [1]. This is a one-dimensional model, which does not show the output. The first transmission-line section represents the waveguide leading up to the bend. The second section represents the impedance that the high dielectric-constant material introduces. The size and position of the high dielectric material determines the electrical length (d_d) of this transmission line. The third section corresponds to the waveguide material between the high dielectric material and the back wall of the waveguide. Likewise, the length (d_s) is dependent on the high dielectric material size. The last section is the free-space impedance seen behind the wall. The goal is to force the reflection coefficient to zero at the input (Γ_{in}) by varying the high dielectric material size, position, and relative permittivity. At the same time, it is desirable to minimize wave transmission to free space (maximize Γ_{so}) so a minimal amount of energy is lost. This reflection coefficient is determined by the difference of the relative permittivity between the waveguide and free space and is given by the following equation [2]:

$$\Gamma_{SO} = \frac{\sqrt{\varepsilon_r} - 1}{\sqrt{\varepsilon_r} + 1}. \tag{1}$$

In order to make the reflection coefficient as large as possible, we want a material with a large dielectric constant. If the energy is not reflected at the input and is not transmitted to free space, it must be captured by the high dielectric material and launched toward the output.

As mentioned above, this model is used for the sole purpose of finding an initial guess for the more rigorous finite difference time domain (FDTD) analysis discussed in Section II-B.

B. Waveguide Analysis Using the FDTD Method

The FDTD method has been known for some time. The Yee algorithm, developed in 1966, is the most widely used FDTD scheme because it is so robust [3]. The Yee algorithm solves for both the electric and magnetic field using the coupled Maxwell's curl equations, rather than solving for one field using the wave equation. This approach has several advantages (including magnetic and electric material properties), which can be modeled easily, and the algorithm can be applied to a wide variety of structures [3]. These reasons made the Yee FDTD algorithm a logical choice in modeling the frequency response of a dielectric waveguide discontinuity.

The perfectly matched layer (PML) absorbing boundary condition (ABC) was introduced by Berenger in 1994. This technique uses a nonphysical medium, which matches the impedance of free space and absorbs electromagnetic energy at any frequency and incidence angle [5]. The PML layer can only absorb the tangential components of waves that are traveling normal to the PML layer. Although the PML has reported 1/3000 times lower reflection than Mur's ABC, it does not work well with evanescent waves. For evanescent waves, the attenuation rate is the same as free space, therefore, to obtain the same reflection magnitude, the number of cells in the PML region must be increased. To overcome this problem, a new method, called the modified PML (MPML), was developed [6]. It provides an extra degree of freedom, which allows the adjusting of the parameters to allow a faster rate of attenuation of evanescent waves [6]. Since dielectric waveguides produce evanescent waves outside the waveguide, the MPML ABC was implemented.

C. Broad-Band Analysis

When the frequency characteristics of a device are needed, it is useful to launch a pulse that has several frequency components, so several simulations at discrete frequencies are not required. Since the Fourier transform of a Gaussian pulse is Gaussian, it contains a continuous set of frequencies, which can be launched in the time domain. The spectral response of the pulse can be placed on a carrier so the response of bandpass structures, such as waveguides, can be found. The equation of a Gaussian pulse modulated on a carrier of ω_o is

$$v(t) = \sin(\omega_o t) \exp\left[-\frac{(t - t_o)^2}{2\sigma^2}\right] \tag{2}$$

where t_o is the pulse delay and σ is the standard deviation of the pulse [8]. In the FDTD algorithm, let $t = n \cdot dt$ and $t_o = b \cdot dt$, where n and b are the time-domain integer counterparts. For a reasonable pulse bandwidth, let

$$\sigma = \frac{b \cdot dt}{4\sqrt{2}}. \tag{3}$$

Placing the Gaussian pulse on a carrier puts the largest amplitude in the center of the frequency band of interest, which will aid in reducing roundoff errors due to the small numbers in the tail of the Gaussian function. In most of the simulations performed, $dt = 0.2407$ ps and $b = 600$ to give a pulse centered at 28.5 GHz and a bandwidth of 32 GHz (see Fig. 2), which is well beyond the expected operating bandwidth of the waveguide structure.

Bootstrapping, also known as the mode template approach, is an important method which allows consistent results by avoiding the possible distortions of the launched Gaussian pulse [9]. The goal is to create a source condition which mimics the actual field distribution from an approximate initial distribution. The advantage is that the computational domain of the simulation can be reduced because the modes are fully developed as they would be in a long waveguide, so the source can be placed near the discontinuity. Also, when an approximation to the field distribution propagates into the mode that is supported, reflections can occur. These reflections are nonphysical and can be eliminated. For this reason, another FDTD simulation is run on a long straight section of dielectric waveguide. The approximate initial distribution used for the dielectric waveguide is a sinusoidal variation $(\sin(\pi x/a))$ of the z-direction electric field in the cross section of the

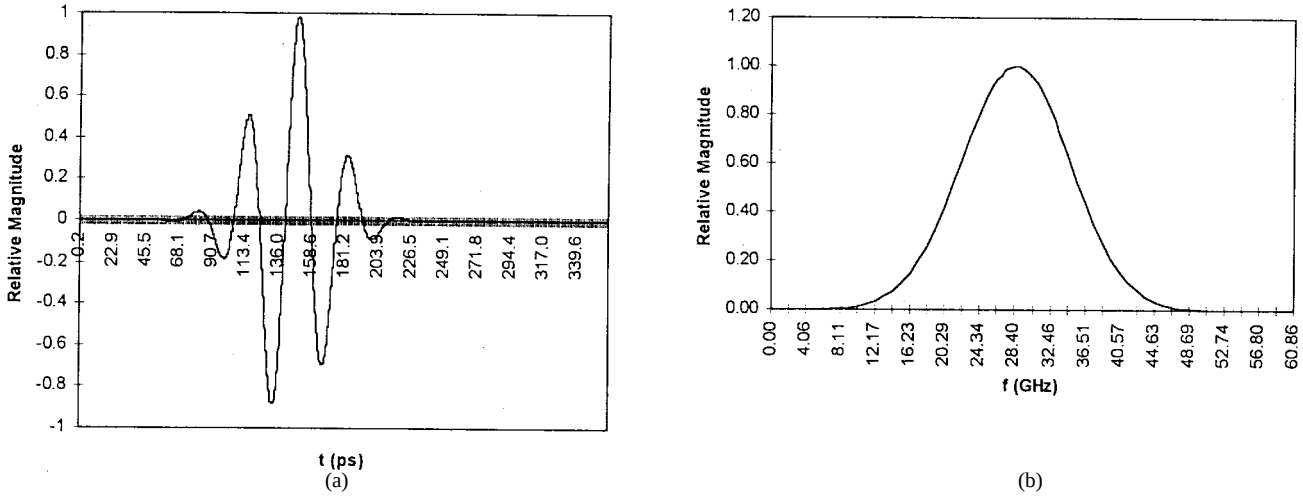

(a) (b)

Fig. 2. Time- and frequency-domain Gaussian shaped pulse used for broad-band analysis.

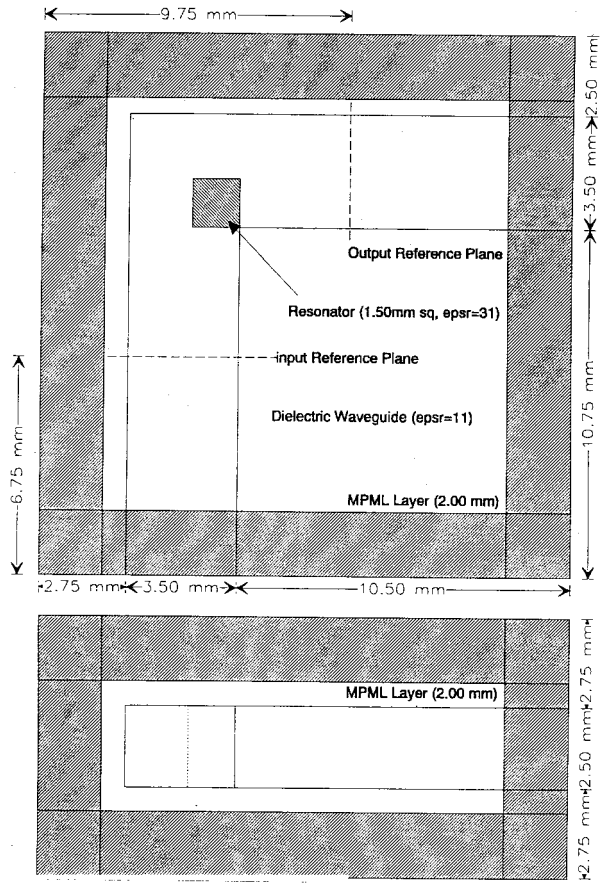

Fig. 3. FDTD computational domain and optimum high dielectric material size and location for the 90°-bend discontinuity for material placed inside waveguide.

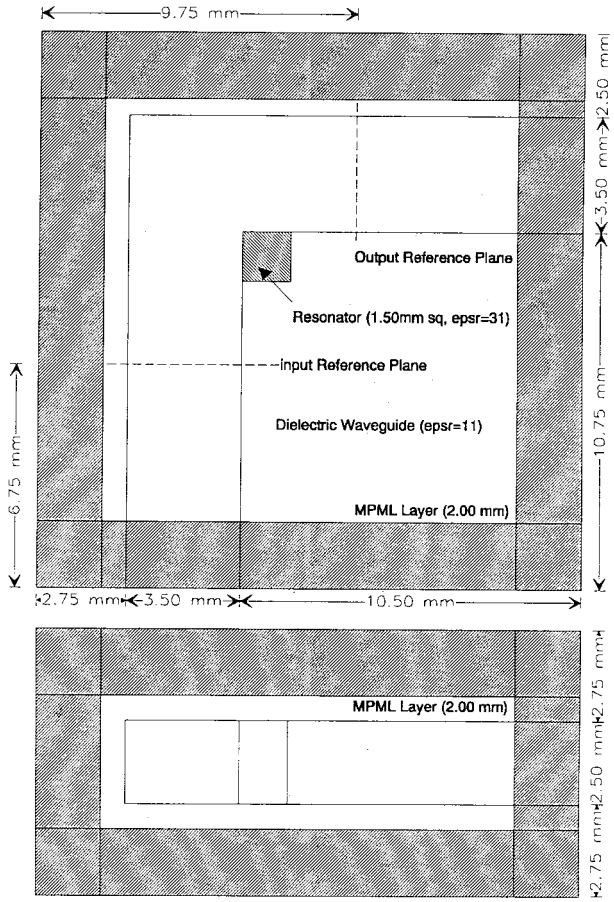

Fig. 4. FDTD computational domain and optimum high dielectric material size and location for the 90°-bend discontinuity for material placed outside waveguide.

waveguide. When the fields are maximum at the output port, the entire field distribution in the output plane is saved. Theoretically, there are not any reflections at the output due to the MPML layer on all six sides of the computational domain. Since this set of data represents the fully developed mode, it is input to the discontinuity simulation and is modulated by the broad-band Gaussian pulse centered at 28.5 GHz. The source condition cannot be placed too close to either the discontinuity or the MPML. Experimentation shows that placing the source about five to six cells from the MPML will not produce noticeable reflections, even without bootstrapping.

D. Power, S-Parameter, and Impedance Calculations

The FDTD algorithm solves for the electric and magnetic fields over the entire computational domain at each time step. From this data, the power and S-parameters can be found as

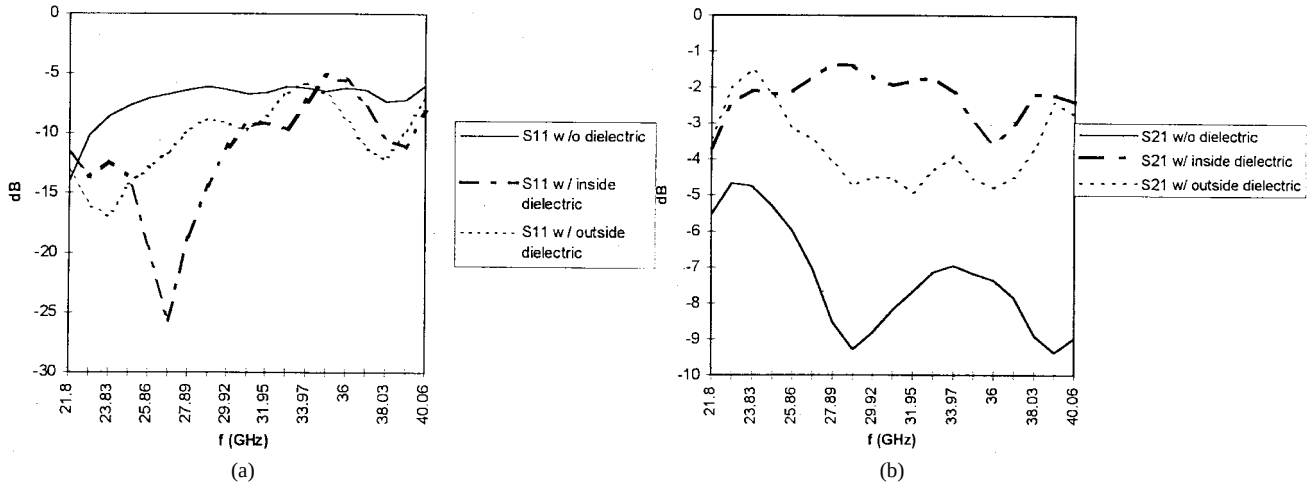

Fig. 5. 90°-bend frequency response.

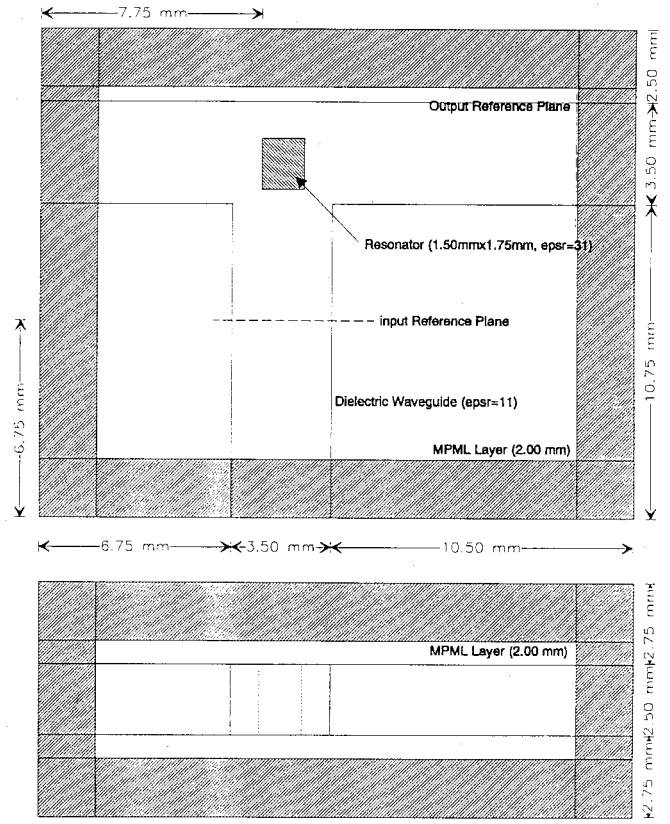

Fig. 6. FDTD computational domain and optimum high dielectric material size and location for the T-junction for material placed inside waveguide.

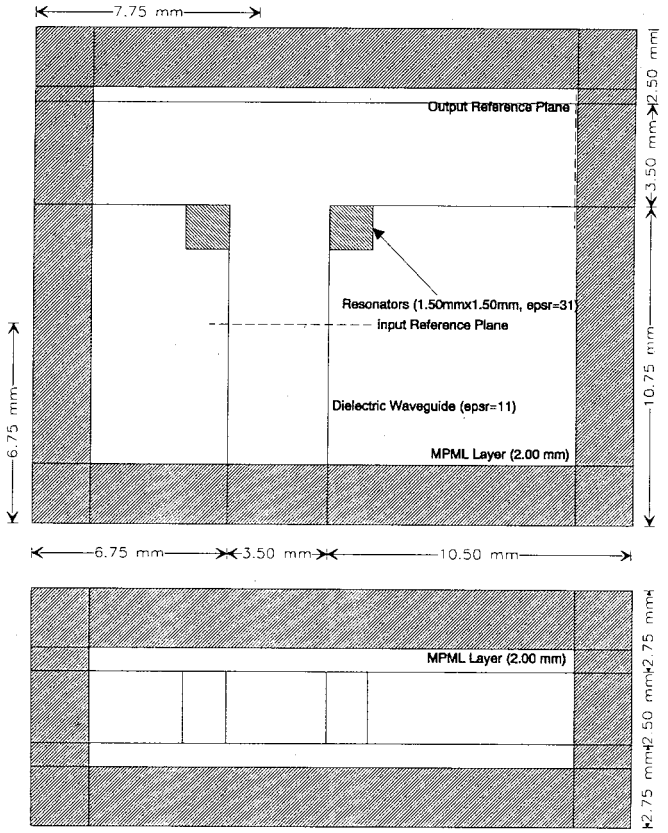

Fig. 7. FDTD computational domain and optimum high dielectric material size and location for the T-junction for material placed outside waveguide.

a function of frequency. Power and S-parameter calculations require reference planes: one at the input and one at the output. All six field components are saved at each time step in both reference planes. Taking the fast Fourier transform (FFT) of each time-varying field component gives the field distribution as a function of frequency. The Poynting vector gives the power at each point, thus, the power in the entire reference plane is

$$P = \tfrac{1}{2} \iint_S \mathrm{Re}(\vec{E}(\omega) \times \vec{H}^*(\omega)) \cdot d\vec{S}. \tag{4}$$

Calculation is not as straightforward as it might seem. Since there is a 1/2-cell difference between the E and H fields, the geometric mean must be used in the appropriate direction [10]. Thus,

$$H_X = \sqrt{H_X(i+0.5, j, k) \cdot H_X(i, j, k)} \tag{5}$$

$$H_Z = \sqrt{H_Z(i, j, k+0.5) \cdot H_Z(i, j, k)}. \tag{6}$$

For an FDTD simulation of a waveguide in the y-direction and accounting for the 1/2-cell difference between the electric and magnetic fields, the integral reduces to

$$P = \tfrac{1}{2} \cdot \Delta x \cdot \Delta z \cdot \sum_x \sum_z E_z(\omega)\, H_x(\omega) - E_x(\omega)\, H_z(\omega). \tag{7}$$

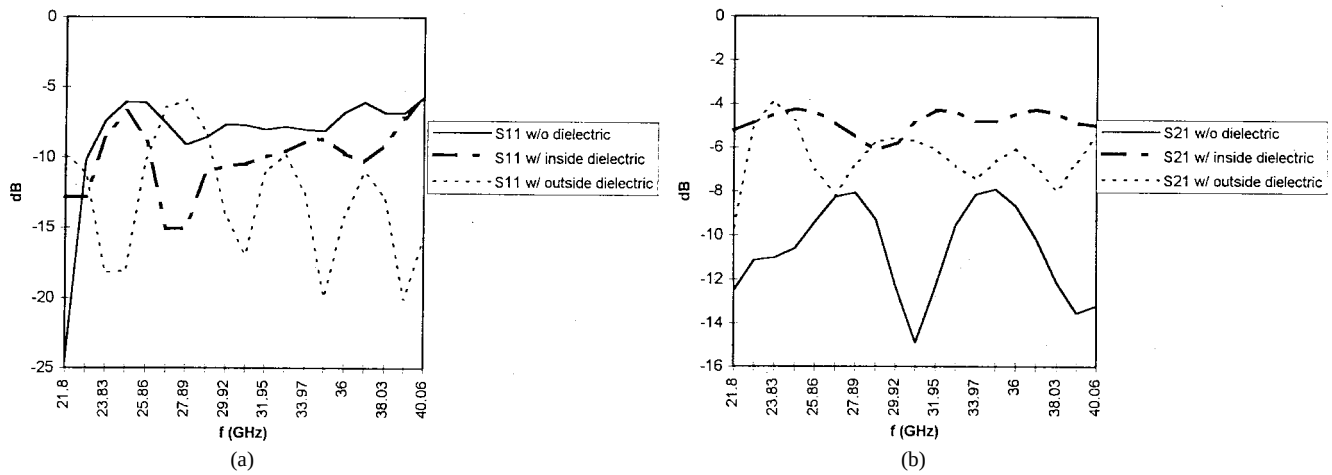

Fig. 8. T-junction frequency response.

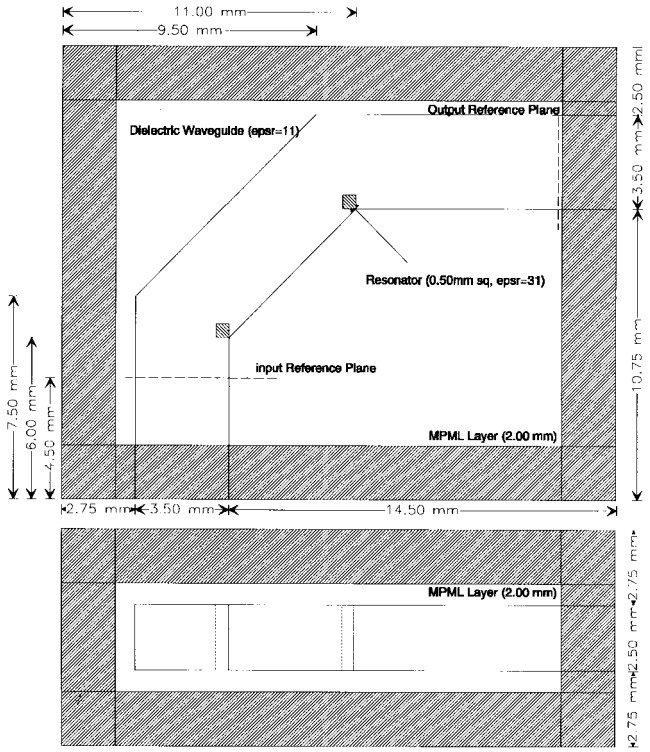

Fig. 9. FDTD computational domain and optimum high dielectric material sized and location for the 45°-bend discontinuity for material placed inside waveguide.

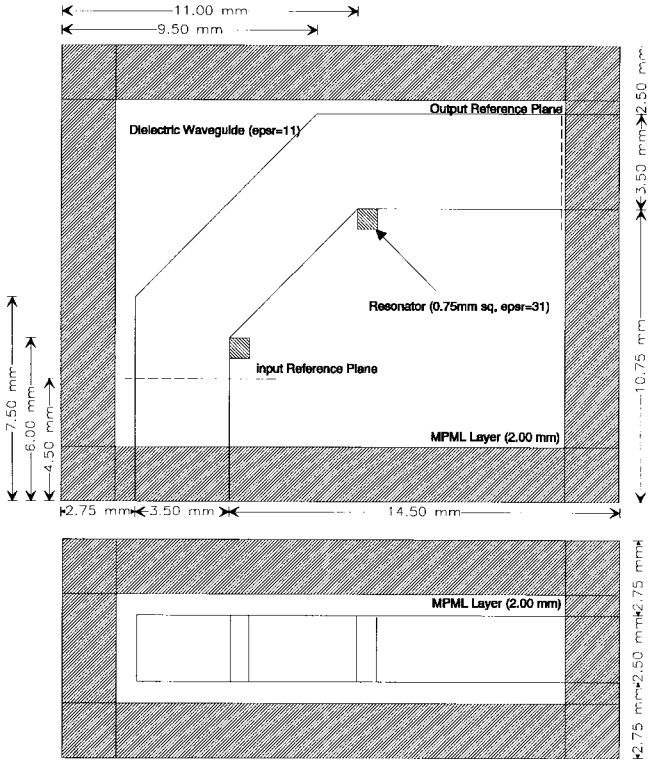

Fig. 10. FDTD computational domain and optimum high dielectric material sized and location for the 45°-bend discontinuity for material placed outside waveguide.

The scattering parameters can be found from the power calculations. There are two popular methods for finding the incident and reflected pulses at the input: subtraction and time windowing. Subtraction allows the reflected pulse to be found by taking the total field at the reference plane and subtracting out the incident pulse that is user defined. By running a simulation and observing the time-domain waveforms, the pulse reflected from the discontinuity can be separated from the incident pulse using time windowing, provided that the source condition was not applied too close to the discontinuity. In this case, the reflected pulse will return to the reference plane after the incident pulse leaves the reference plane. The output should never see a reflection because it is terminated into an MPML region. Once the incident and reflected pulses are separated at the input reference plane, the FFT and the Poynting vector summation can be used independently to find their respective frequency-domain powers. The S-parameters are calculated using the following well-known equations:

$$|S_{11}| = 10 \cdot \log\left(\frac{P_r}{P_i}\right)$$

and

$$|S_{21}| = 10 \cdot \log\left(\frac{P_o}{P_i}\right). \tag{8}$$

In a similar manner, the wave impedance can be calculated. Since the time-domain data is known, the impedance at each point can be calculated. If the dielectric waveguide is directed

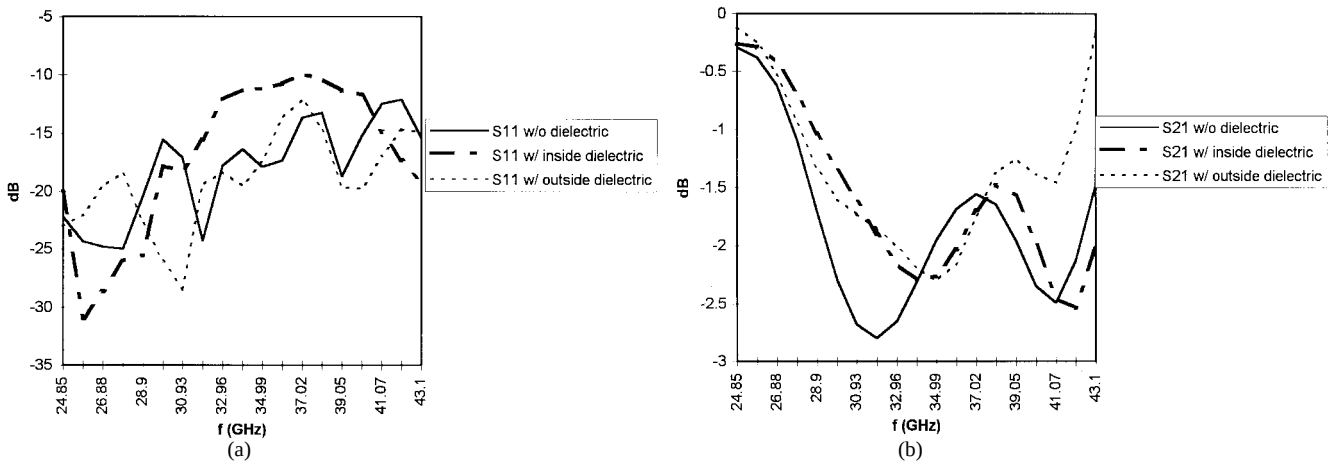

(a) (b)

Fig. 11. 45°-bend frequency response.

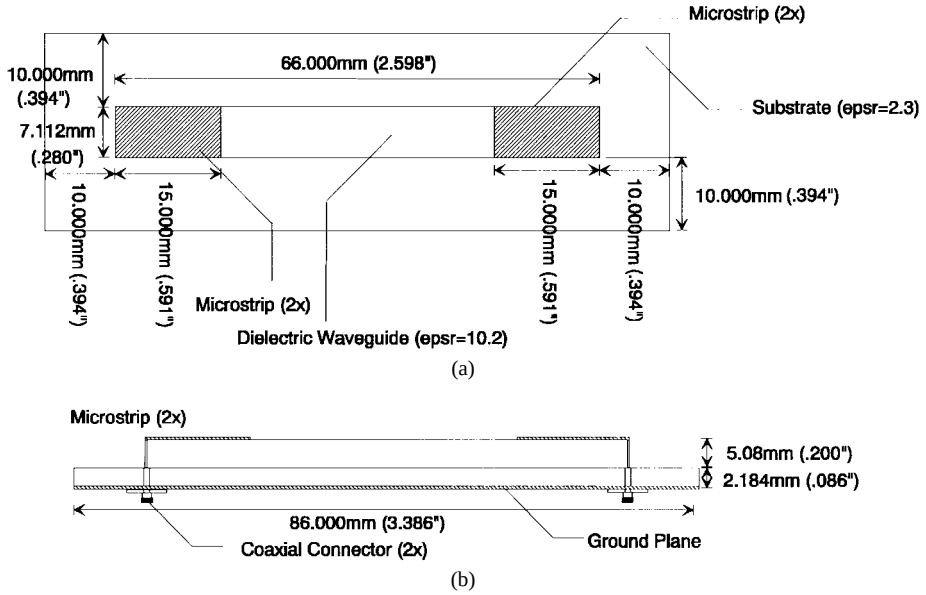

(a)

(b)

Fig. 12. Calibration waveguide with microstrip excitation.

in the y-direction, the wave impedance is [2]

$$Z_w^{+y} = \frac{-E_x}{H_z} = \frac{E_z}{H_x}. \tag{9}$$

Since the data obtained from bootstrapping is fully developed, it can be used to calculate the impedance. This is actually preferred because the data is generated from a straight section of waveguide, which is numerically infinite due to the MPML ABC.

E. Optimization

Since there is freedom to choose the size and location of the high dielectric material for a given waveguide discontinuity, there needs to be a method to optimize these parameters. The goal of this paper is to reduce the loss seen by a dielectric waveguide discontinuity, thus S_{21} is used as the figure-of-merit. Rather than concentrating on the maximum value of S_{21} of a specified frequency band, a statistical measure, which is the root-mean-square (rms) value of S_{21}, over the bandwidth is maximized. A simple three-point optimization technique where the maximum value of $S_{21\mathrm{rms}}$ is stored along with the high dielectric material size and position.

III. Simulation Results: Effects of High Dielectric Material

A. Introduction

The FDTD algorithm was applied to three discontinuities: the 90° bend, the T-junction, and the 45° bend. Bootstrapping was used in every case to help obtain accurate results. Simulation of each structure focused on the S-parameter versus frequency response and its improvement with the insertion of the high dielectric material. An optimization is used in every case to maximize the rms value of the insertion loss. A substantial improvement is seen with a carefully selected dielectric size and location.

B. The 90° Bend

The 90°-bend simulations were performed with and without the dielectric material. Due to the symmetry and reciprocity of the bend, the optimization of the high dielectric material

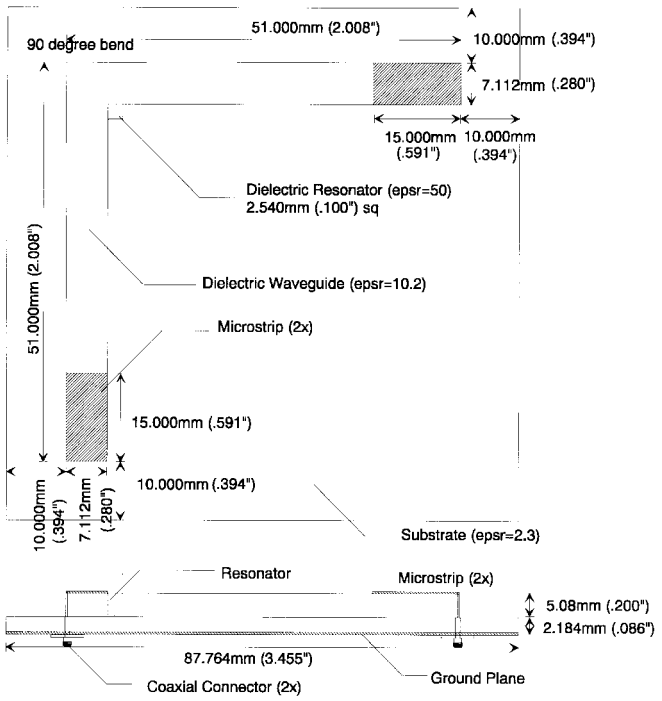

Fig. 13. 90°-bend waveguide with microstrip excitation.

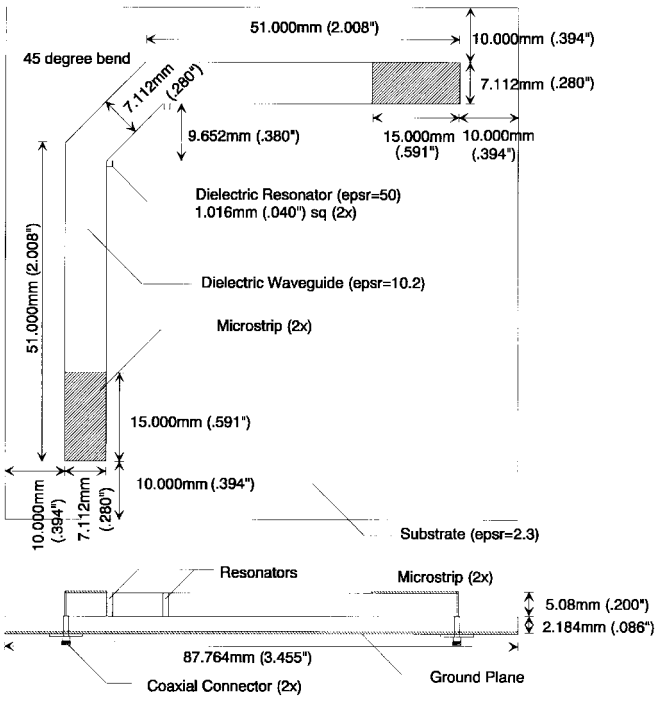

Fig. 14. 45°-bend waveguide with microstrip excitation.

for minimum insertion loss is limited to the diagonal of the corner. Since the structure is easier to manufacture with the high dielectric material placed outside the waveguide, this case was also optimized. Figs. 3 and 4 shows the FDTD computational domain, discontinuity dimensions, and optimum dielectric size and location along the plane of symmetry for both the inside and outside cases. The FDTD cell size is 0.25 mm, thereby limiting the dielectric to integer multiples of this cell size. A 0.25-mm cell size is a good balance between

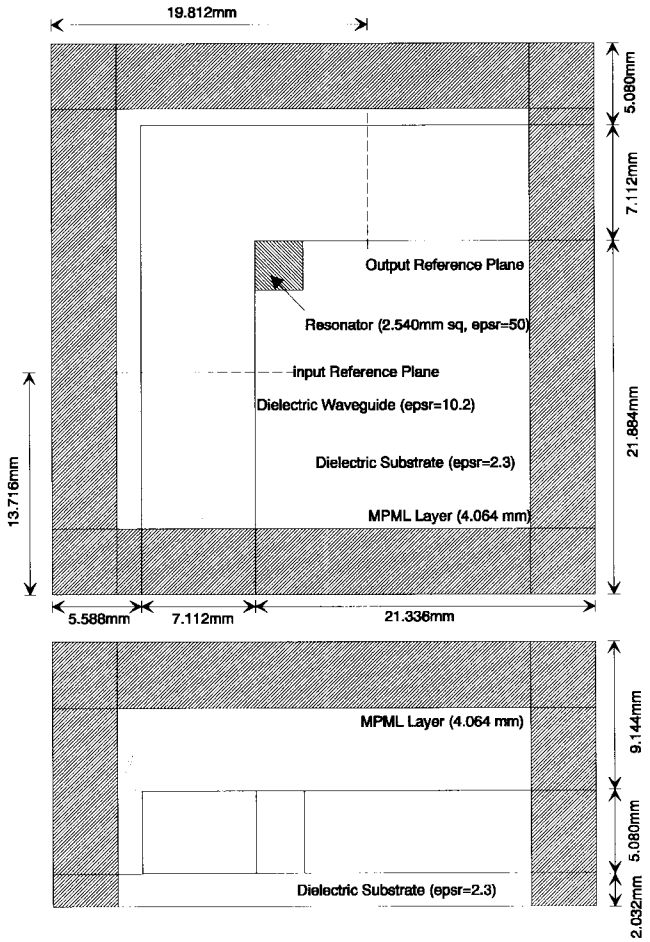

Fig. 15. FDTD computational domain and resonator size and location for the 90°-bend test structure.

required memory and wavelength. The highest frequency used in the simulations was 43 GHz, which has a wavelength of 2.1 mm, giving about eight cells per wavelength. Without the high dielectric the structure suffers from large losses at the discontinuity (see Fig. 5), providing an rms insertion loss of 7.1 dB over the desired frequency band of 21.8–40.0 GHz. The optimum position of the high dielectric material has been found to be at the inside corner of the discontinuity. This tends to equalize the phase of the signal along different path of the waveguide, including a discontinuity. An optimum 1.50-mm-square dielectric material with $\varepsilon_r = 31$ placed at the inside corner (see Fig. 3) will provide an rms insertion loss of 2.2 dB, an improvement of 4.9-dB rms, and tends to make the frequency response flatter (see Fig. 5). The same dielectric placed outside the waveguide on the inside corner (see Fig. 4), has an rms insertion loss of 3.5 dB (see Fig. 5), an improvement of 3.6 dB over the case without a dielectric.

C. The T-Junction

The T-junction simulations were performed for a high dielectric material placed along the plane of symmetry. In this case, the high dielectric material was not required to be square because symmetry is lost from the input to output ports. However, the high dielectric material was optimized along the plane of symmetry to guarantee that both output

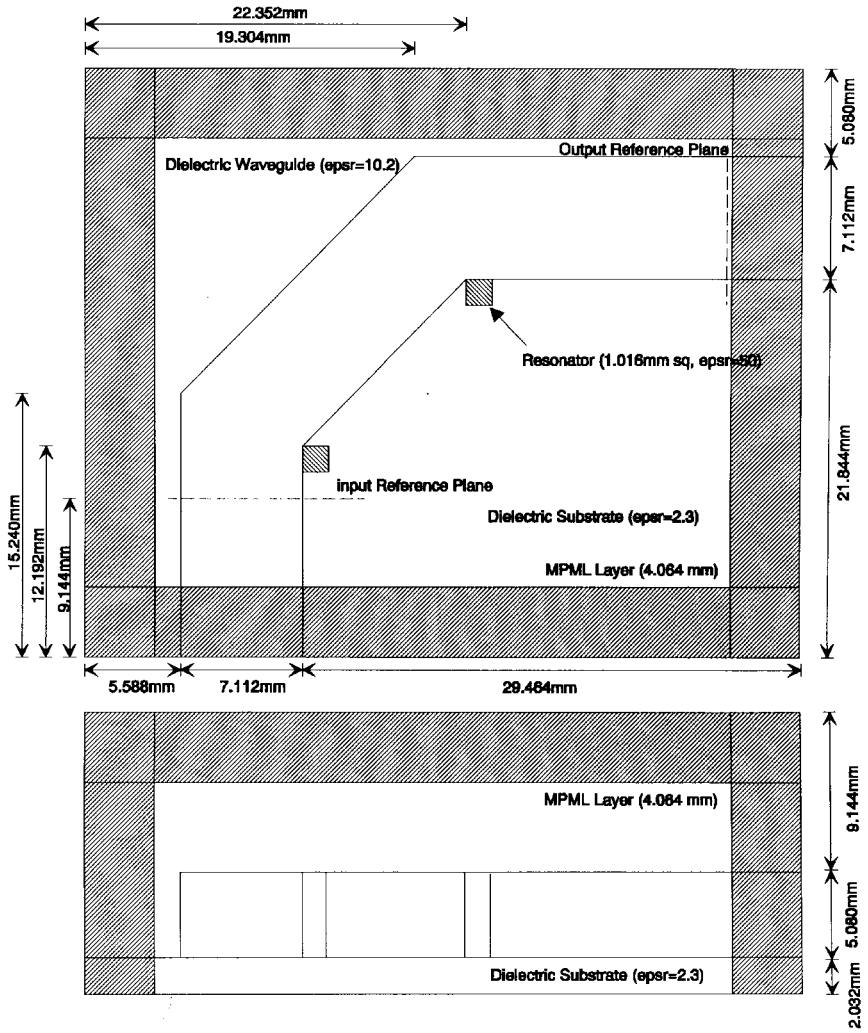

Fig. 16. FDTD computational domain and resonator size and location for the 45°-bend test structure.

ports would see the same insertion loss. Figs. 6 and 7 show the FDTD computational domain, T-junction dimensions, and optimum high dielectric material size and location. The rms insertion loss without a high dielectric material is 10.2 dB (see Fig. 8). The optimum high dielectric material dimensions are 1.50 mm $\times$ 1.75 mm. A substantial improvement is seen with the optimized solution; an rms insertion loss of 4.8 dB over the frequencies of 21.8–40.0 GHz and the frequency response is smoother (see Fig. 8). With the high dielectric material placed outside the waveguide, the rms insertion loss improved by 4.0 dB (see Fig. 8) and the response is flatter. Note that the minimum insertion loss of a T junction is approximately 3.5 dB. The power is split evenly between the two output ports, resulting in a 3-dB loss. Also, there is an impedance mismatch at the discontinuity. Looking from the input port, the output ports are in parallel with the same characteristic impedance. This provides a reflection coefficient of

$$\Gamma = \frac{Zo - \dfrac{Zo}{2}}{Zo + \dfrac{Zo}{2}} = \frac{1}{3}. \tag{10}$$

The ratio of maximum transmitted power at one output port is $0.5(1 - \Gamma^2) = 4/9 = -3.5$ dB. Thus, with the high dielectric material, the predicted losses are 1.3 dB higher than the minimum theoretical limit.

D. The 45° Bend

The 45° transition is used to soften the impact of discontinuity. However, this bend is more complicated in design and optimization and requires more space than the 90° bend. Simulations were performed with and without the high dielectric materials. During optimization of the insertion loss, the high dielectric material was confined to the plane of symmetry both inside and outside the waveguide. Optimization also includes the length of the 45° bend. Figs. 9 and 10 show the FDTD computational domain, discontinuity dimensions, and optimum high dielectric material size and locations along the plane of symmetry for both the inside and outside case. Without the high dielectric material, an optimized 45° bend has a reasonably flat frequency response (see Fig. 11), providing an rms insertion loss of 1.7 dB over the 24.8–43.1-GHz frequency band. An improvement of the rms insertion loss is seen when the size and location of the high dielectric material is optimized for locations inside the waveguide. An optimum 0.50-mm-square high dielectric material placed at the inside corner will provide an rms insertion loss of 1.5 dB, an improvement of

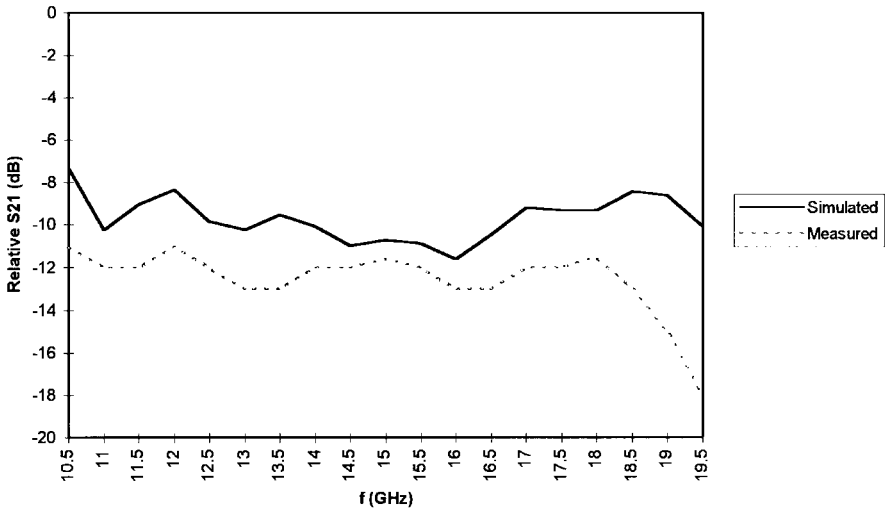

(a)

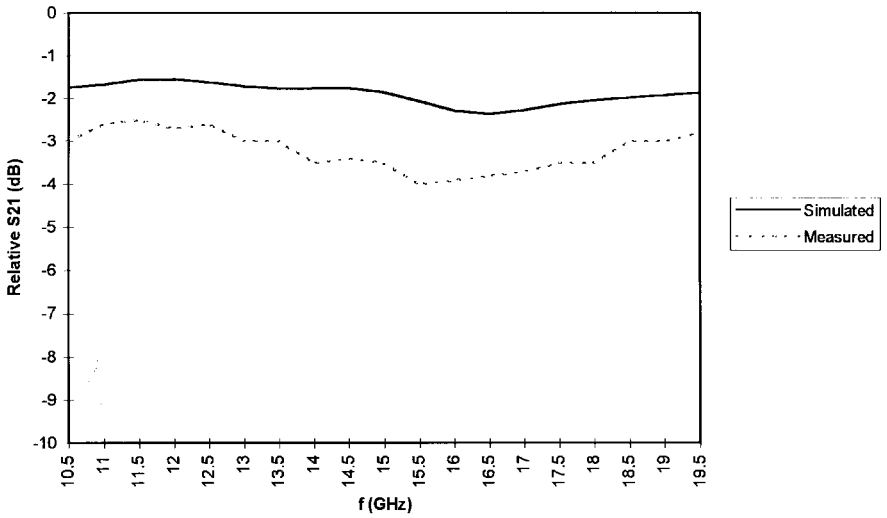

(b)

Fig. 17. Measured and simulated results for the (a) 90° bend and (b) 45° bend. Frequency response with substrate and without high dielectric material.

0.2 dB rms and tends to make the frequency response flatter (see Fig. 11). An optimum 0.75-mm-square high dielectric material placed outside the waveguide on the inside corner has an rms insertion loss of 1.3 dB (see Fig. 11). In this case, the lowest insertion loss (0.4-dB improvement) is seen with the high dielectric material placed outside the waveguide, which is easier to manufacture.

IV. Experimental Verification

A. Introduction

The preceding discussion found the insertion loss as a function of frequency for the 90° and 45° bend. To test the structures, an interface to the waveguide is required. A substrate with a ground plane was added to provide a microstrip interface between the waveguide and a coaxial cable used on a network analyzer. The microstrip is used as a quarter-wave transformer between the 50-Ω cable and the 95-Ω waveguide, which requires a transformer impedance of $\sqrt{50 \cdot 95} = 69\ \Omega$. In the interest of time, Maxwell, a two-dimensional field solver, was used to iteratively solve the waveguide–substrate cross section for the appropriate width of the microstrip to provide 69 Ω and the phase velocity of the infinite structure.

B. Building the Test Structures

In order to eliminate the effects of the coaxial and microstrip interface, a calibration structure was built (see Fig. 12). It is a straight section of waveguide with the same dimensions, quarter-wave transformers, and substrate as the 90° and 45° bends. The straight section is preferred because there is relatively little insertion loss. The waveguide section is simply glued to the substrate and coaxial connectors are connected to the top microstrip line to excite the waveguide. The 90° bend (see Fig. 13) was assembled in a similar manner. The bend is made up of two sections of straight waveguide glued together at the bend. The 45° bend (see Fig. 14) is made up of three sections. In each case, a straight section of approximately three wavelengths is provided before and after the discontinuities to allow the modes to be fully developed before the discontinuity and to provide consistent results with the calibration structure.

C. Test Results and Simulation Comparison

The insertion loss of the 90° and 45° bends were measured using an HP8510 network analyzer. Measurements were performed without the high dielectric materials due to the lack of availability of the appropriate-size high dielectric materials. Furthermore, the difference in insertion loss in the 45° bend is fairly small. As stated earlier, the calibration structure's purpose is to eliminate the effects of the microstrip interface. Sweeps were performed for the calibration structure, 90° bend, and the 45° bend from 10.5 to 19.5 GHz. Simulations were performed with the structures discontinuity dimensions. Due to the large memory requirement and the fact that it could be calibrated out, the microstrip interface was not simulated. Also, since the input signal was bootstrapped in the simulations and the straight sections have very low loss, the full length of the straight sections in the test structures for the 45° and 90° bends were not required. Figs. 15 and 16 show the computational domain for the test structures.

The relative insertion loss of the 90° bend without the high dielectric material (see Fig. 17) show excellent correlation. Notice that the general trend is very close, but is shifted down about 2 dB. This discrepancy is due to joint (glued connection) and conductor (ground plane) losses that were not modeled.

Similar results were found in the 45° case (see Fig. 17). The conductor and joint losses shifted the measured curve down about 1.5-dB rms, but showed the same trends. The difference between measured and simulated insertion loss is between 0.9 and 1.9 dB.

V. Conclusion

This paper used the FDTD method to investigate the improvement of insertion loss by adding a high dielectric material near a dielectric waveguide discontinuity, as well as smooth transition at the discontinuity. Three types of discontinuities were optimized with respect to the rms insertion loss: the 90° bend, the T-junction, and the 45° bend. For each discontinuity, a high dielectric material was placed in the discontinuity and an optimization was performed to find the size and position of the high dielectric material that provided the lowest rms insertion loss over the frequencies of interest. For the 90° and 45° bend, the high dielectric material was also optimized for size when the high dielectric material was placed outside the waveguide and against the inside corner of the discontinuity. In order to validate the simulation results, two cases were studied and tested: the 90° and 45° bend placed on a substrate.

Computer simulations showed that the 90° bend has an rms insertion-loss improvement of 4.9 dB over the 21.8–40.0-GHz band when the high dielectric material is placed inside the waveguide. With the high dielectric material placed outside the waveguide, the insertion loss is improved by 3.6 dB. The high dielectric material also has another desirable effect: it tends to flatten the frequency response. Similarly, the T-junction's insertion loss is improved by 5.4 dB with the optimum high dielectric material placed inside the waveguide. The 45° bend showed the smallest improvement, largely due to its low loss without a high dielectric material. An improvement of 0.4 dB is demonstrated when the high dielectric material is placed outside the waveguide.

The 90° and 45° bends with a substrate were simulated with the same material and dimensions as the structure which was tested. Results show excellent correlation between measured and simulated results, thus validating the method and simulation tool.

References

[1] E. A. El-Sharawy and P. A. Tirkas, "A novel design to reduce losses at dielectric waveguide discontinuities," in *IEEE Microwave Theory Tech. Symp. Dig.*, vol. 2, Orlando, FL, May 23–27, 1995, pp. 841–844.

[2] C. A. Balanis, *Advanced Engineering Electromagnetics.* New York: Wiley, 1989.

[3] A. Taflove, *Computational Electrodynamics.* Norwood, MA: Artech House, 1995.

[4] G. Mur, "Absorbing boundary conditions for the finite-difference approximation of the time-domain electromagnetic-field equations," *IEEE Trans. Electromag. Compat.*, vol. EMC-23, pp. 377–382, Nov. 1981.

[5] J. P. Berenger, "A perfectly matched layer for the absorption of electromagnetic waves," *J. Comput. Phys.*, vol. 114, pp. 185–200, 1994.

[6] B. Chen, D. G. Fang, and B. H. Zhou, "Modified Berenger PML absorbing boundary condition for FD-TD meshes," *IEEE Microwave Guided Wave Lett.*, vol. 5, pp. 399–401, Nov. 1995.

[7] D. Katz, E. T. Thiele, and A. Taflove, "Validation and extension to three dimensions of the Berenger PML absorbing boundary condition for FD-TD meshes," *IEEE Microwave Guided Wave Lett.*, vol. 4, pp. 268–270, Aug. 1994.

[8] C. W. Helstrom, *Probability and Stochastic Processes for Engineers.* New York: Macmillan, 1991.

[9] C. J. Railton and J. P. McGeehan, "The use of mode templates to improve the accuracy of the finite difference time domain method," in *Proc. European Microwave Conf.*, Stuttgart, Germany, 1991, pp. 12 781–12 785.

[10] J. Fang and D. Xeu, "Numerical errors in the computation of impedance by FDTD method and ways to eliminate them," *IEEE Microwave Guided Lett.*, vol. 5, pp. 6–8, Jan. 1995.

Robert Elio was born in Tucson, AZ, on October 27, 1967. He received the M.S. degree in electrical engineering from Arizona State University, Tempe, in 1996, and is currently working toward the Ph.D. degree.

He is currently a Design Engineer in the Semiconductor Products Sector, Motorola, Chandler, AZ. His main research interest is FDTD analysis.

El-Badawy El-Sharawy received the B.Sc. with honors and M.Sc. degrees from Mansoura University, Mansoura, Egypt, in 1980 and 1984, respectively, and the Ph.D. degree from the University of Massachusetts, Amherst, in 1989.

In 1989, he joined Arizona State University, Tempe, where he is currently an Associate Professor of electrical engineering. His research interests are in the area of microwave circuits, applied electromagnetics, anisotropic devices, and cellular-phone antennas.

Dr. El-Sharawy is a member of the IEEE MTT-13 Technical Committee and an elected member of Commissions A and D, National URSI.